

Electronic Supplementary Information

Alkyl chain engineering of pyrene fused perylene diimides: impact on the transport ability, and microfibers self-assembly

Xuejun Zhan,^{1#} Ji Zhang,^{2#} Yanbin Gong,¹ Sheng Tang,¹ Jin Tu,¹ Yujun Xie,¹ Qian Peng,² Gui Yu,^{*2} and Zhen Li^{*1}

¹Department of Chemistry, Hubei Key Lab on Organic and Polymeric Opto-Electronic Materials, Wuhan University, Wuhan, 430072, China.

E-mail: lizhen@whu.edu.cn or lichemlab@163.com

²Institute of Chemistry, the Chinese Academy of Sciences, Beijing, China.

E-mail: yugui@iccas.ac.cn

[#]The authors contributed equally to this work.

Table of Contents

1. **Scheme 1.** Synthesis of the pyrene fused PDIs bearing different alkyl chains.
2. **Chart S1.** Some examples showing the importance of alkyl chain length (A), branching point (B) and alkyl chain modification (C).
3. **Figure S1.** DSC curves of the DPPDIs.
4. **Figure S2.** Phase transition temperatures and melt points of the DPPDI-R.
5. **Figure S3.** Calculated UV spectrum of DPPDI core.

6. **Table S1.** Absorption wavelengths and oscillator strength of DPPDI evaluated by the TD-DFT (B3LYP/6-311G (d, p)) calculation.
7. **Figure S4.** Transfer and output characteristics of (a, e) DPPDI-R1, (b, f) DPPDI-R2, (c, g) DPPDI-R3, (d, h) DPPDI-R4, (i, m) DPPDI-R5, (j, n) DPPDI-R6, (k, o) DPPDI-R7 and (l, p) DPPDI-R8.
8. **Figure S5.** XRD pattern of the thin films of DPPDI-R at room temperature.
9. **Table S2.** Detailed OFET performance of the DPPDI-R5 annealed at different temperature.
10. **Figure S6.** AFM images of thin films of DPPDI-R5 annealed at different temperature: (a) pristine; (b) 80 °C; (c) 120 °C; (d) 160 °C; (e) 200 °C; (f) 240 °C.
11. **Figure S7-S14.** ¹H NMR and ¹³C NMR spectra of the DPPDI-R(1-8).
12. **Figure S15-22.** HRMS (MALDI-TOF) spectrum of DPPDI-R(1-8).

Experimental Section

THF was dried over and distilled from K-Na alloy under an atmosphere of argon. All other chemicals and reagents were purchased from commercial suppliers and used without further purification unless otherwise specified. Most of the ¹H and ¹³C NMR spectra were measured on a Varian Mercury 300 with TMS as an internal standard (the attached ¹H NMR spectra of DPPDI-R1, DPPDI-R2 and DPPDI-R7 were measured on Varian Inova 600). Elemental analyses of carbon, hydrogen, and nitrogen were performed on a CARLOERBA-1106 microanalyzer. HRMS spectra were recorded on a GCT premier CAB048 mass spectrometer operating in MALDI-TOF (matrix-assisted laser desorption/ionization-time-of-flight) mode with *trans*-2-[3-(4-*tert*-butylphenyl)-2-methyl-2-propenylidene] malononitrile (DCTB) as the matrix. UV-vis absorption spectra were recorded on a Shimadzu UV-2500 recording spectrometer. Photoluminescence spectra were recorded on a Hitachi F-4500 fluorescence spectrometer. Thermogravimetric analysis (TGA) was undertaken with a NETZSCH STA 449C instrument. The thermal stability of the samples under a nitrogen atmosphere was determined by measuring their weight loss while heating at a rate of 10 °C min⁻¹ from 25 to 800 °C. Differential scanning calorimetry

(DSC) was measured on a Mettler Toledo DSC 822e at a heating rate of 10 °C min⁻¹ from room temperature to 450 °C under nitrogen. Cyclic voltammetry (CV) was carried out on a CHI voltammetric analyzer in a three-electrode cell with a Pt counter electrode, a Ag/AgCl reference electrode, and a glassy carbon working electrode at a scan rate of 100 mVs⁻¹ with 0.1 M tetrabutylammonium perchlorate (purchased from Alfa Aesar) as the supporting electrolyte, in anhydrous dichloromethane solution purged with nitrogen. The potential values obtained in reference to the Ag/Ag⁺ electrode were converted to values versus the saturated calomel electrode (SCE) by means of an internal ferrocenium/ferrocene (Fc⁺/Fc) standard. The X-ray diffraction (XRD) measurements were carried out using D/max 2500 X-Ray Diffractometer, with scan scale from 2 ° to 30 °, 5 °/min. The atomic force microscope (AFM) measurements were carried out using Veeco Nanoscope IV, tapping mode. The geometrical and electronic properties were optimized at B3LYP/6-31g (d) level using Gaussian 09 program. Meanwhile, the molecular orbitals were obtained at the same level of theory.

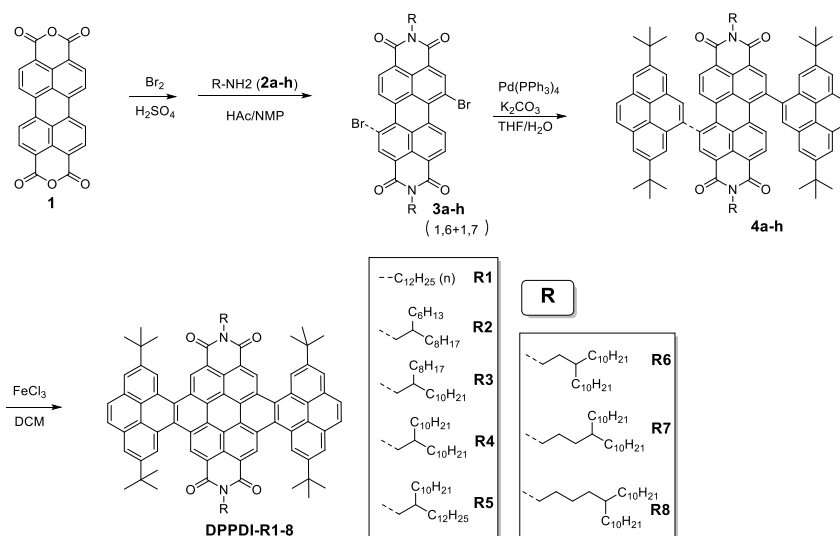
Devices Fabrication

OTFT devices were fabricated in a bottom-contact configuration. Before the deposition of organic semiconductors, source and drain electrodes made of gold were pre-prepared on the SiO₂/Si substrates. The octyltrichlorosilane (OTS) treatment was performed on the gate dielectrics, which were placed in a vacuum oven with OTS at a temperature of 120 °C to form an OTS self-assembled monolayer. Then the thin films were spin-coated on the OTS modified SiO₂/Si substrates from the chloroform solutions. The OTFTs characteristics of the devices were determined at room temperature in air by using a Keithley 4200 SCS. The mobility of the devices was calculated in the saturation regime. The equation is listed as follows:

$$I_{DS} = (W / 2L) C_i \mu (V_{GS} - V_{th})^2$$

where W/L is the channel width / length, C_i is the insulator capacitance per unit area, and V_{GS} and V_{th} are the gate voltage and threshold voltage, respectively.

Synthesis



Scheme 1. Synthesis of the pyrene fused PDIs bearing different alkyl chains.

General procedure for the synthesis of PDI-2Br (**3a-h**)¹

A mixture of perylene-3,4,9,10-tetracarboxylic acid bisanhydride (**1**, 10.0 g, 25.50 mmol) and H₂SO₄ (98 wt%, 40 mL) was stirred at room temperature for 12 h. I₂ (260 mg, 1.02 mmol) was then added, the mixture was heated to 85 °C with vigorous stirring for 30 min. Then bromine (8.16 g, 51.10 mmol) was added dropwise over a time period of 3 h, and the reaction mixture was stirred for 16 h at 85 °C. After being cooled to room temperature, the mixture was poured into ice (100 g). The precipitate was filtered, washed with sulfuric acid (50%, 100 mL) and then a large amount of H₂O until neutral. The residue was dried to give a red powder. The crude product was used for the next step directly.

A suspension of brominated perylene bisanhydrides (5.00 g) obtained in the above reaction, compounds **2a-h** (29.5 mmol), and acetic acid (3.0 mL) in *N*-methyl-2-pyrrolidinone (125 mL) was stirred at 85 °C under N₂ for 12 h. After the mixture was cooled to room temperature, the precipitate was separated by filtration, washed with MeOH (250 mL), and dried in a vacuum. The crude product was purified by silica gel column chromatography to give compounds **3a-h** as black solids. It should be noted that 1,6-PDI-2Br and 1,7-PDI-2Br could not be separated by column chromatography.

General procedure for the synthesis of **4a-h**

A mixture of (2,7-di-(*tert*-butyl)pyren-4-yl)-4,4,5,5-tetramethyl-1,3,2-dioxaborolane (210 mg, 0.48 mmol),² compound **3a-h** (0.16 mmol), Pd(PPh₃)₄ (30 mg) and potassium carbonate (440 mg, 3.2 mmol) in THF (10 mL) and distilled water (1.6 mL) was refluxed for 24 h under nitrogen in a Schlenk tube. The mixture was extracted with dichloromethane. The combined organic extracts were dried over anhydrous Na₂SO₄ and concentrated by rotary evaporation. The crude product was purified by column chromatography on silica gel using dichloromethane/petroleum ether as eluent to afford the product as black solid in the yield of about 75%. However, the mixture of **1,6-PDI-Pyrene** and **1,7-PDI-Pyrene** could not be separated and was used directly in the next step.

General procedure for the synthesis of DPPDI-R

A solution of compound **4a-h** in dichloromethane was degassed for 20 min in an ice bath. The solution was bubbled with N₂ in the whole experiment. Then anhydrous FeCl₃ in CH₃NO₂ was slowly added by syringe. After being stirred for 30 min at 0 °C, the reaction was stirred for another 1 h at room temperature. Quenched by methanol, the solvent was removed by rotary evaporation and the residue was purified by column chromatography on silica gel to give the target compound **DPPDI-R** as a red solid. In this step, due to the symmetry of the molecule, no isomers existed.

DPPDI-R1. 85% yield. ¹H NMR (600 MHz, CDCl₃) δ (ppm): 11.06 (s, 4H), 9.45 (s, 4H), 8.43 (s, 4H), 8.21 (s, 4H), 4.53 (t, *J* = 7.2 Hz, 4H), 1.96 (m, 8H), 1.75 (s, 36H), 1.44-1.24 (m, 32H), 0.84 (t, *J* = 7.2 Hz, 6H). ¹³C NMR (75 MHz, CDCl₃) δ (ppm): 165.2, 149.3, 131.1, 131.0, 129.1, 127.6, 127.5, 127.1, 126.5, 123.9, 123.6, 123.5, 123.2, 122.3, 121.2, 44.9, 36.8, 35.5, 31.8, 30.0, 29.7, 29.5, 29.2, 26.6, 26.5, 22.6, 22.5, 14.0, 13.9. HRMS (MALDI-TOF, *m/z*): 1347.7894 ([M⁺], calcd for C₉₆H₁₀₂N₂O₄, 1346.7840). Anal. Calcd for C₉₆H₁₀₂N₂O₄: C, 85.55; H, 7.63; N, 2.08. Found: C, 85.32; H, 8.83; N, 2.12.

DPPDI-R2. 76% yield. ¹H NMR (600 MHz, CDCl₃) δ (ppm): 11.04 (s, 4H), 9.45 (s, 4H), 8.42 (s, 4H), 8.21 (s, 4H), 4.45 (d, *J* = 6.6 Hz, 4H), 2.23 (m, 2H), 1.74 (s, 36H), 1.50-1.13 (m, 48H), 0.80 (t, *J* = 7.2 Hz, 6H), 0.72 (t, *J* = 7.2 Hz, 6H). ¹³C NMR (75 MHz, CDCl₃) δ (ppm): 164.8, 149.3, 131.1, 130.9, 129.1, 127.7, 127.6, 127.1, 126.5, 124.0, 123.6, 123.5, 123.2, 122.3, 121.2, 40.8,

35.5, 31.9, 31.8, 29.6, 29.5, 29.4, 29.3, 28.3, 27.2, 22.6, 14.0. HRMS (MALDI-TOF, m/z): 1459.9166 ($[M^+]$, calcd for $C_{104}H_{118}N_2O_4$, 1458.9092). Anal. Calcd for $C_{104}H_{118}N_2O_4$: C, 85.55; H, 8.15; N, 1.92. Found: C, 85.27; H, 8.29; N, 2.08.

DPPDI-R3. 74% yield. 1H NMR (300 MHz, $CDCl_3$) δ (ppm): 11.11 (s, 4H), 9.48 (s, 4H), 8.48 (s, 4H), 8.28 (s, 4H), 4.50 (d, $J = 7.8$ Hz, 4H), 2.21 (m, 2H), 1.76 (s, 36H), 1.51-1.08 (m, 64H), 0.73 (m, 12H). ^{13}C NMR (75 MHz, $CDCl_3$) δ (ppm): 165.1, 149.2, 131.0, 131.0, 130.9, 129.0, 127.6, 127.1, 126.5, 123.9, 123.8, 123.5, 123.1, 122.2, 121.1, 44.7, 36.7, 35.5, 35.4, 31.8, 31.8, 31.7, 30.0, 29.9, 29.6, 29.5, 29.5, 29.2, 29.1, 26.6, 22.5, 22.4, 13.9. HRMS (MALDI-TOF, m/z): 1572.0281 ($[M^+]$, calcd for $C_{112}H_{134}N_2O_4$, 1571.0344). Anal. Calcd for $C_{112}H_{134}N_2O_4$: C, 85.56; H, 8.59; N, 1.78. Found: C, 85.31; H, 8.84; N, 1.67.

DPPDI-R4. 64% yield. 1H NMR (300 MHz, $CDCl_3$) δ (ppm): 11.12 (s, 4H), 9.48 (s, 4H), 8.48 (s, 4H), 8.28 (s, 4H), 4.50 (d, $J = 5.4$ Hz, 4H), 2.22 (m, 2H), 1.76 (s, 36H), 1.51-1.09 (m, 72H), 0.74 (t, $J = 7.2$ Hz, 12H). ^{13}C NMR (75 MHz, $CDCl_3$) δ (ppm): 165.1, 149.3, 131.1, 130.9, 129.0, 127.6, 127.5, 127.1, 126.5, 123.9, 123.6, 123.5, 123.2, 122.3, 121.1, 44.8, 36.7, 35.5, 31.8, 31.7, 30.0, 29.7, 29.6, 29.5, 29.2, 26.6, 22.5, 13.9. HRMS (MALDI-TOF, m/z): 1628.1075 ($[M^+]$, calcd for $C_{116}H_{142}N_2O_4$, 1627.0970). Anal. Calcd for $C_{116}H_{142}N_2O_4$: C, 85.56; H, 8.79; N, 1.72. Found: C, 85.28; H, 9.01; N, 1.83.

DPPDI-R5. 68% yield. 1H NMR (300 MHz, $CDCl_3$) δ (ppm): 11.1 (s, 4H), 9.49 (s, 4H), 8.48 (s, 4H), 8.27 (s, 4H), 4.50 (d, $J = 7.2$ Hz, 4H), 2.23 (m, 2H), 1.76 (s, 9H), 1.26 (m, 80H), 0.81 (m, 12H). ^{13}C NMR (75 MHz, $CDCl_3$) δ (ppm): 165.0, 149.2, 131.0, 130.9, 129.0, 127.5, 127.0, 126.5, 123.8, 123.5, 123.1, 122.2, 121.0, 44.8, 36.7, 35.5, 31.8, 31.7, 30.0, 29.6, 29.5, 29.4, 29.2, 29.1, 26.6, 22.5, 14.0, 13.9. HRMS (MALDI-TOF, m/z): 1684.1658 ($[M^+]$, calcd for $C_{120}H_{154}N_2O_4$, 1683.1596). Anal. Calcd for $C_{120}H_{154}N_2O_4$: C, 85.36; H, 9.19; N, 1.66. Found: C, 85.21; H, 9.34; N, 1.67.

DPPDI-R6. 71% yield. 1H NMR (300 MHz, $CDCl_3$) δ (ppm): 11.12 (s, 4H), 9.49 (s, 4H), 8.48 (s, 4H), 8.28 (s, 4H), 4.56 (m, 4H), 1.86 (m, 2H), 1.77 (s, 36H), 1.43-1.17 (m, 76H), 0.81 (t, $J = 7.2$ Hz, 12H). ^{13}C NMR (75 MHz, $CDCl_3$) δ (ppm): 164.7, 149.3, 131.1, 130.9, 129.1, 127.7, 127.6, 127.1, 126.5, 124.0, 123.6, 123.2, 122.3, 121.2, 35.9, 35.5, 33.7, 32.0, 31.8, 30.1, 29.8, 29.7,

29.6, 29.2, 26.6, 22.5. HRMS (MALDI-TOF, m/z): 1656.1343 ($[M^+]$, calcd for $C_{118}H_{146}N_2O_4$, 1655.1283). Anal. Calcd for $C_{118}H_{146}N_2O_4$: C, 85.56; H, 8.88; N, 1.69. Found: C, 85.33; H, 9.14; N, 1.80.

DPPDI-R7. 61% yield. 1H NMR (600 MHz, $CDCl_3$) δ (ppm): 11.06 (s, 4H), 9.45 (s, 4H), 8.41 (s, 4H), 8.19 (s, 4H), 4.52 (t, $J = 6.6$ Hz, 4H), 1.95 (m, 2H), 1.75 (s, 36H), 1.27-1.14 (m, 80H), 0.80 (t, $J = 7.2$ Hz, 12H). ^{13}C NMR (75 MHz, $CDCl_3$) δ (ppm): 164.8, 149.3, 131.1, 130.9, 127.6, 127.1, 126.5, 124.0, 123.6, 123.5, 123.2, 122.3, 121.2, 41.3, 37.3, 35.5, 33.5, 31.8, 31.7, 31.0, 30.1, 29.6, 29.5, 29.2, 26.6, 25.2, 22.5, 14.0. HRMS (MALDI-TOF, m/z): 1684.1638 ($[M^+]$, calcd for $C_{120}H_{150}N_2O_4$, 1683.1596). Anal. Calcd for $C_{120}H_{150}N_2O_4$: C, 85.56; H, 8.98; N, 1.66. Found: C, 85.30; H, 9.23; N, 1.77.

DPPDI-R8. 77% yield. 1H NMR (300 MHz, $CDCl_3$) δ (ppm): 11.11 (s, 4H), 9.48 (s, 4H), 8.48 (s, 4H), 8.28 (s, 4H), 4.55 (m, 4H), 1.92 (m, 2H), 1.77 (s, 36H), 1.35-1.17 (m, 84H), 0.82 (m, 12H). ^{13}C NMR (75 MHz, $CDCl_3$) δ (ppm): 164.7, 149.3, 131.0, 130.9, 129.0, 127.6, 127.1, 126.4, 123.9, 123.5, 123.4, 123.1, 122.2, 121.1, 41.0, 37.4, 35.5, 33.6, 33.5, 31.9, 31.8, 30.1, 29.6, 29.5, 29.2, 28.8, 26.7, 24.4, 22.6, 14.0. HRMS (MALDI-TOF, m/z): 1712.2085 ($[M^+]$, calcd for $C_{122}H_{154}N_2O_4$, 1711.1909). Anal. Calcd for $C_{122}H_{154}N_2O_4$: C, 85.56; H, 9.06; N, 1.64. Found: C, 85.29; H, 9.34; N, 1.85.

- 1 W. Jiang, Y. Li, W. Yue, Y. Zhen, J. Qu and Z. Wang, *Org. Lett.*, 2010, **12**, 228.
- 2 A. C. Bédard, A. Vlassova, A. C. Hernander-Perez, A. Bessette, G. S. Hanan, M. A. Heuft and S. K. Collins, *Chem. Eur. J.*, 2013, **19**, 16295.

p type			
n	mobility (cm ² V ⁻¹ s ⁻¹)	I _{on} /I _{off}	V _T (V)
5	0.43	10 ⁸	-21
6	0.45	10 ⁸	-25
7	0.84	10 ⁷	-29
8	1.80	10 ⁷	-17
9	0.61	10 ⁸	-21
10	0.86	10 ⁸	-23
11	1.76	10 ⁷	-20
12	1.71	10 ⁸	-20
13	2.75	10 ⁷	-27
14	0.72	10 ⁸	-18

A

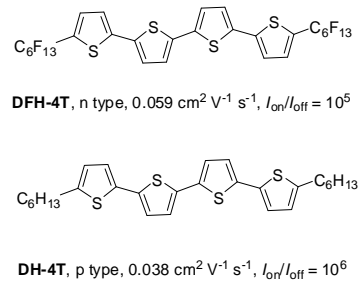
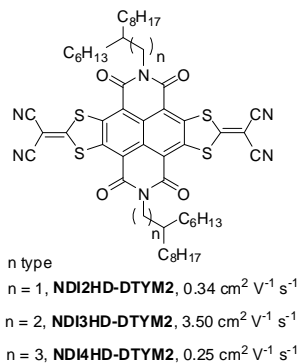


Chart S1. Some examples showing the importance of alkyl chain length (A), branching point (B) and alkyl chain modification (C).

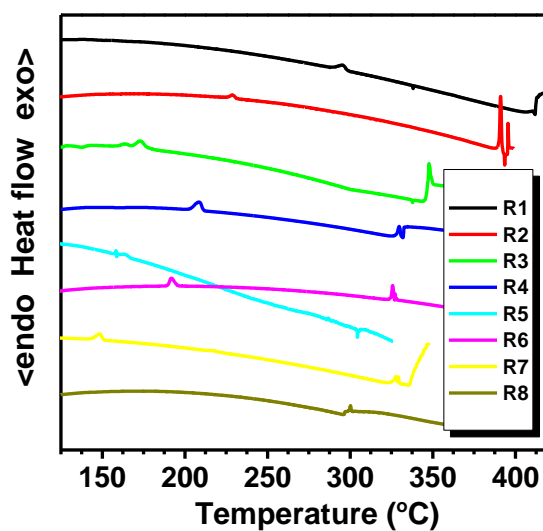


Figure S1. DSC curves of the DPPDIs.

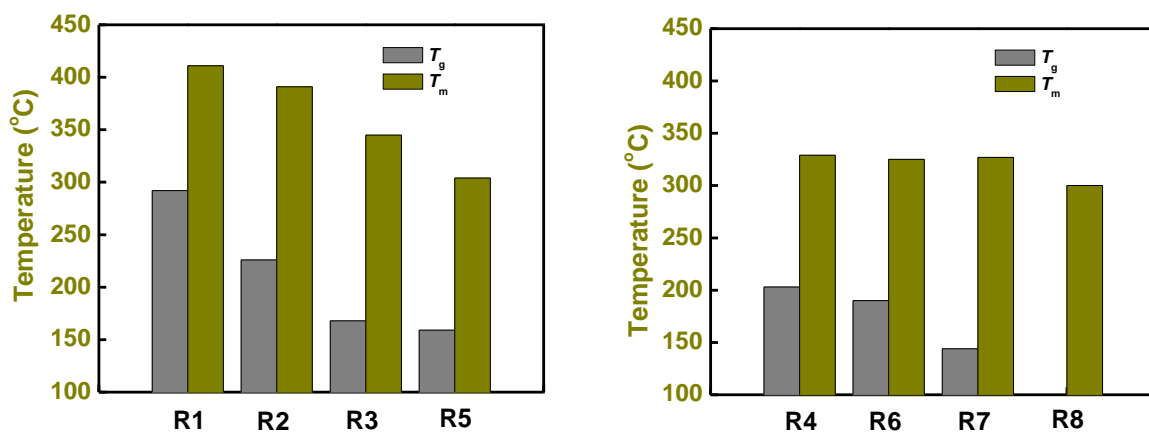


Figure S2. Phase transition temperatures and melt points of the DPPDI-R.

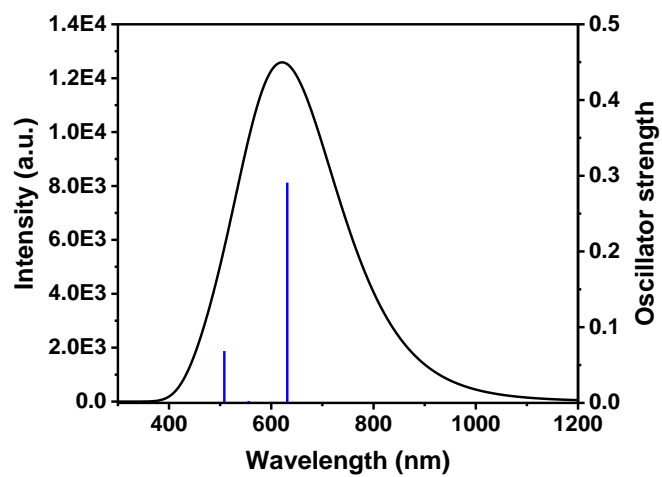


Figure S3. Calculated UV spectrum of DPPDI core.

Table S1. Absorption wavelengths and oscillator strength of DPPDI evaluated by the TD-DFT (B3LYP/6-311G (d, p)) calculation.

Excitation energies	Absorption[nm] (oscillator strength)	Assignments (%)
1.96 eV	631.33 (0.2909)	HOMO→LUMO (98)
2.23 eV	555.81 (0.0025)	HOMO-1→LUMO (99)
2.44 eV	508.19 (0.0685)	HOMO-2→LUMO (87)
		HOMO-1→LUMO+1 (10)

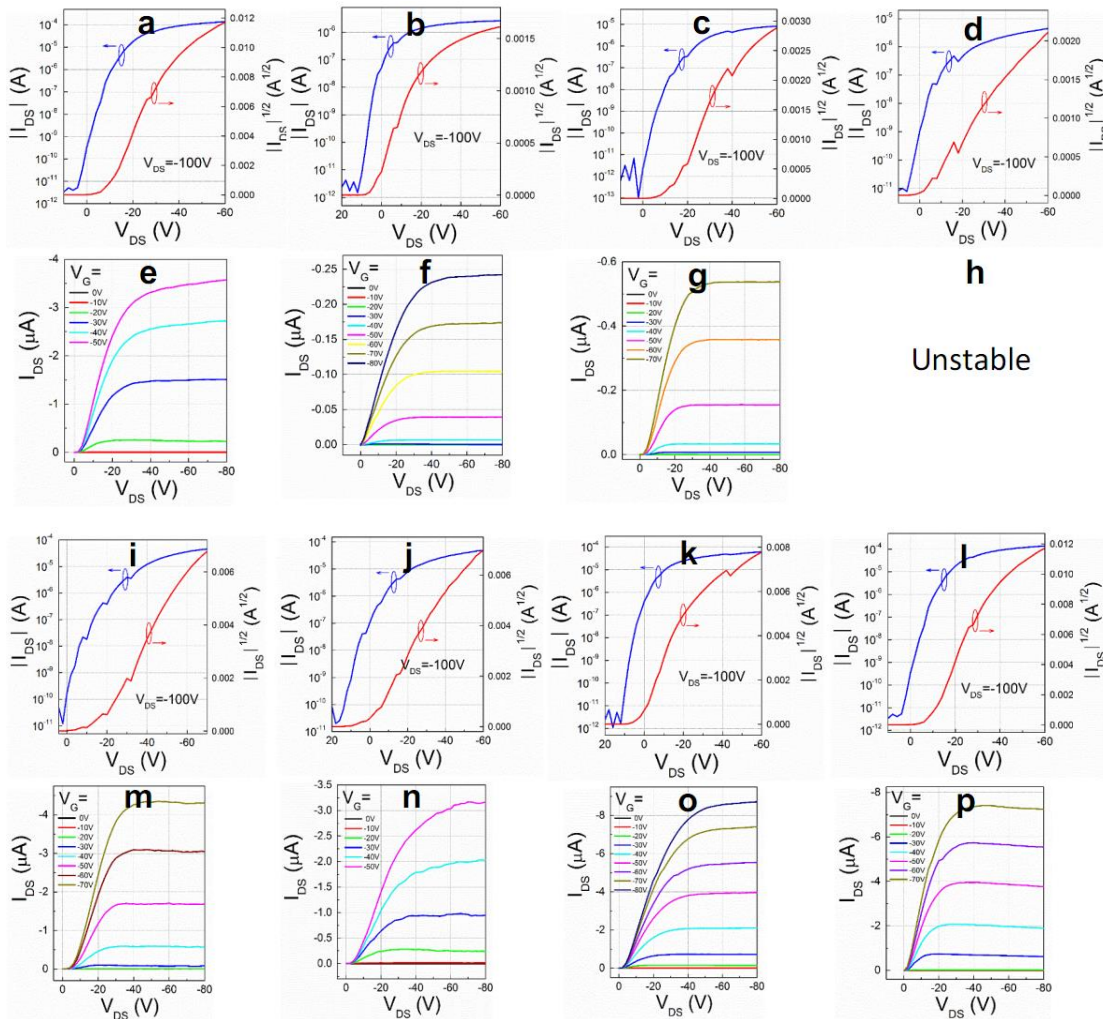


Figure S4. Transfer and output characteristics of (a, e) DPPDI-R1, (b, f) DPPDI-R2, (c, g) DPPDI-R3, (d, h) DPPDI-R4, (i, m) DPPDI-R5, (j, n) DPPDI-R6, (k, o) DPPDI-R7 and (l, p) DPPDI-R8.

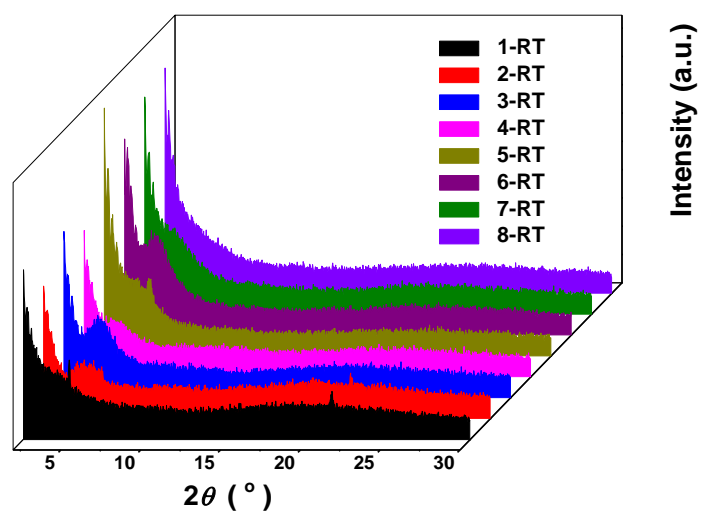


Figure S5. XRD pattern of the thin films of DPPDI-R at room temperature.

Table S2 Detailed OFET performance of the DPPDI-R5 annealed at different temperature.

	$T_{\text{annealing}} [^{\circ}\text{C}]$					
	RT	80	120	160	200	240
$\mu [\text{cm}^2 \cdot \text{V}^{-1} \cdot \text{s}^{-1}]$	1.8E-5 ~7.2E-5	6.0E-5 ~1.34E-4	0.18~0.29	0.84~1.13	0.33~0.64	
$\lg(I_{\text{on}}/I_{\text{off}})$	3—4	3—4	5—7	7—8	6—7	
$V_{\text{threshold}} [\text{V}]$	-25~-26	-23~-44	-4~-10	-9~-10	-15~-24	

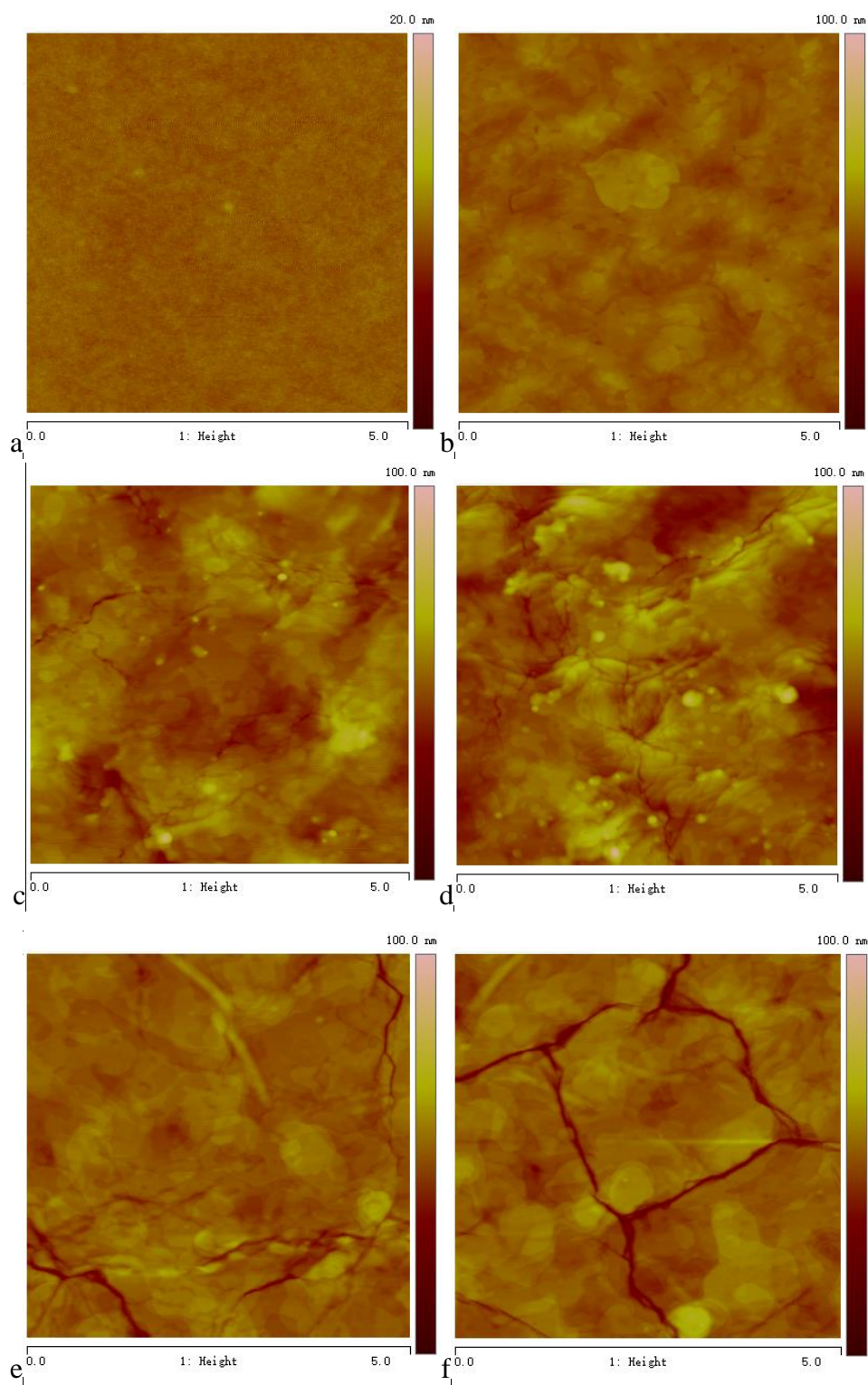


Figure S6. AFM images of thin films of DPPDI-R5 annealed at different temperature: (a) pristine; (b) 80 °C; (c) 120 °C; (d) 160 °C; (e) 200 °C; (f) 240 °C.

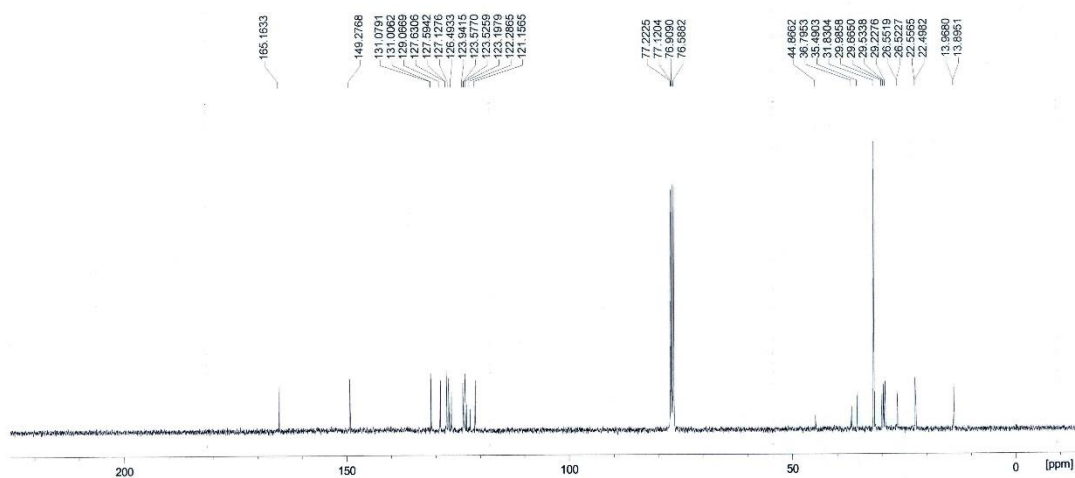
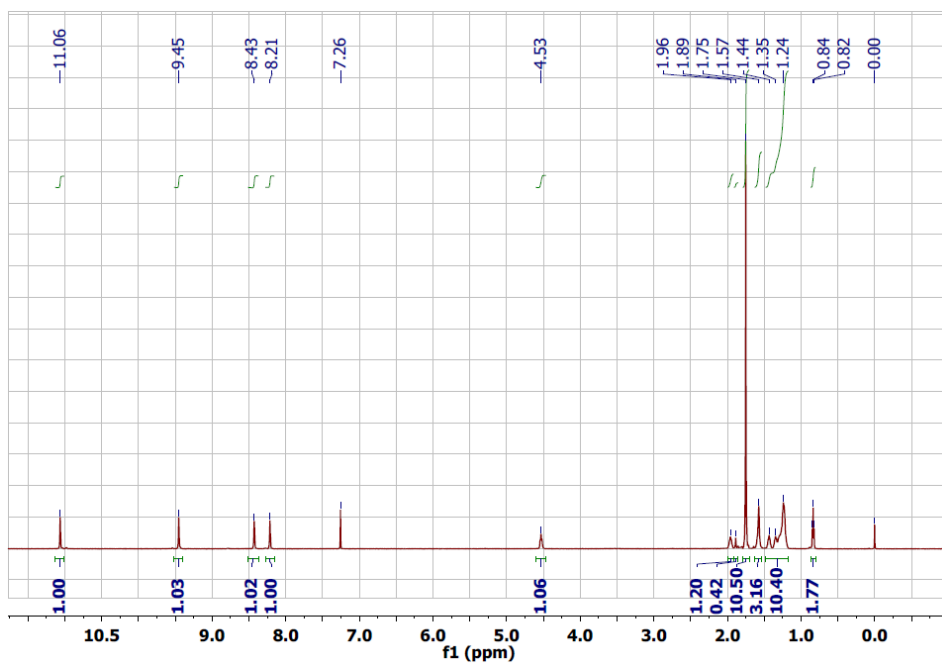
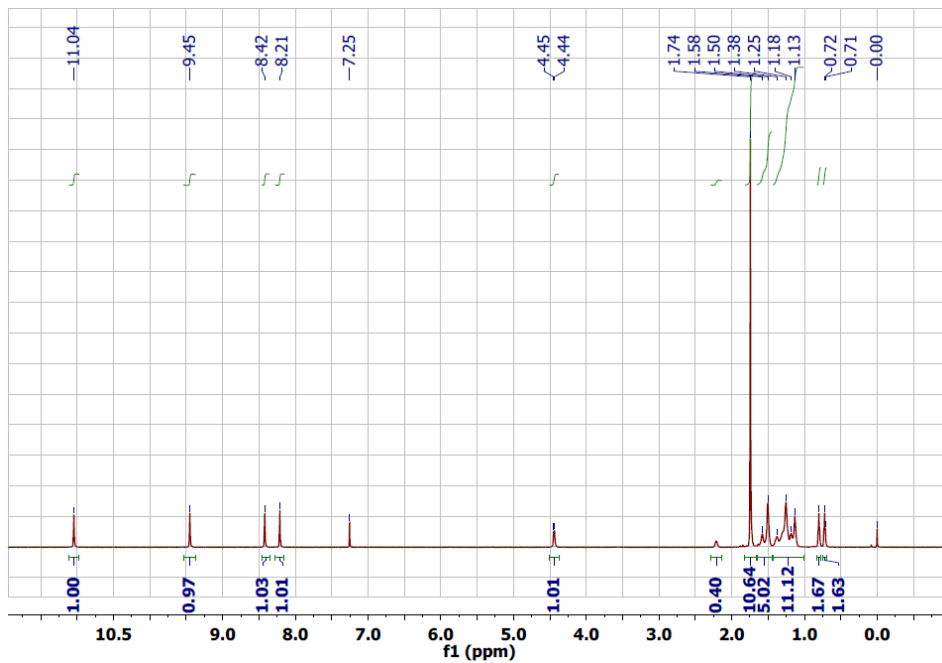


Figure S7. ^1H NMR and ^{13}C NMR spectra of the DPPDI-R1.



27-

ZXJ160317-2-C

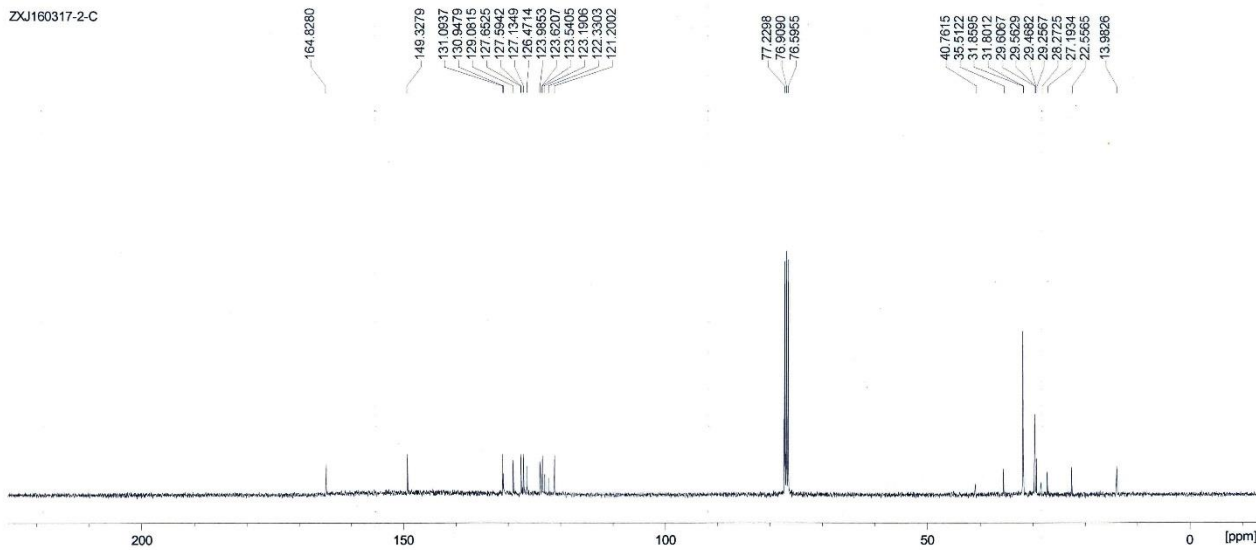
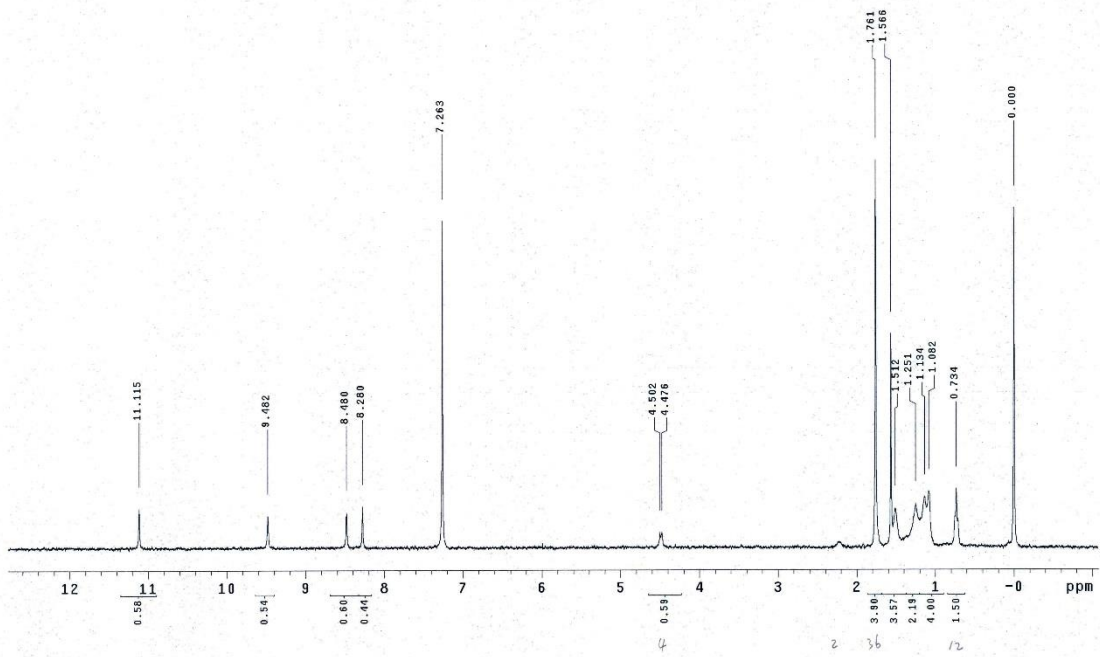


Figure S8. ^1H NMR and ^{13}C NMR spectra of the DPPDI-R2.

278-1



278-1

ZXJ160317-3-C

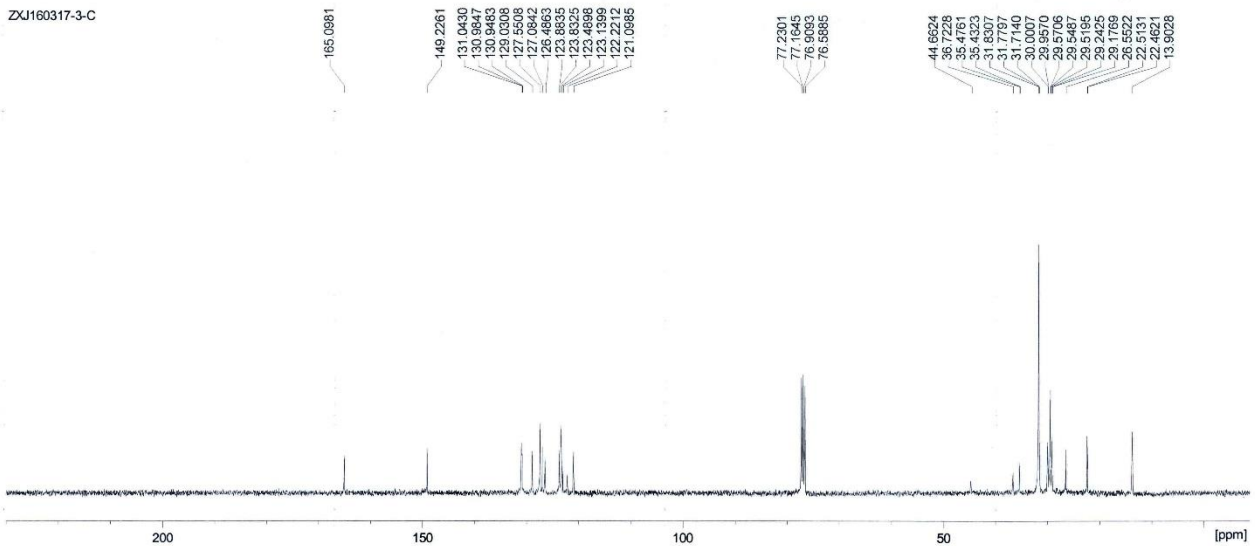
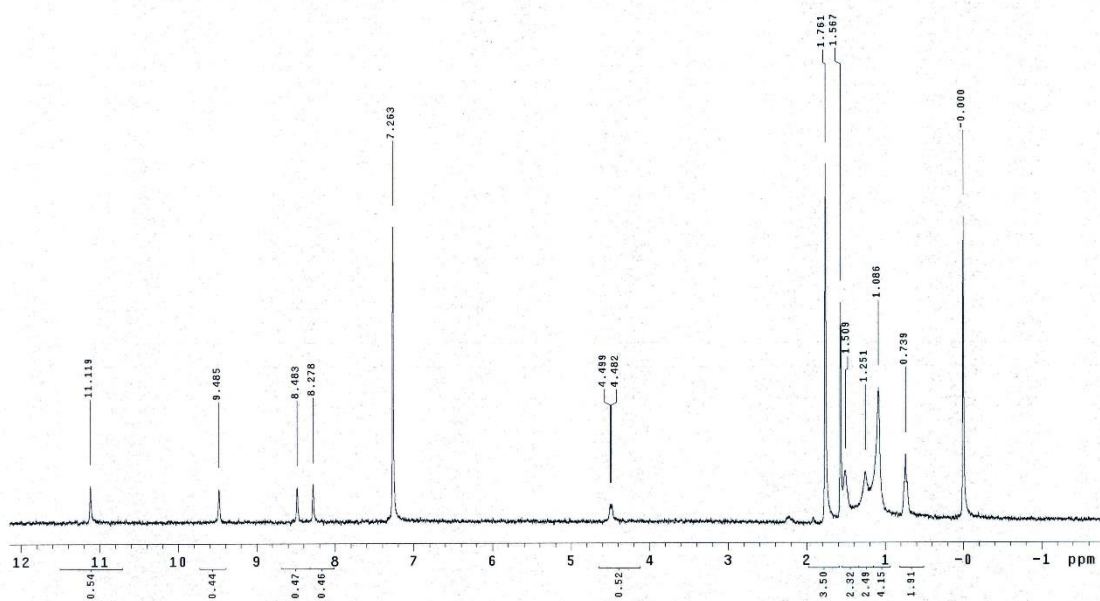


Figure S9. ¹H NMR and ¹³C NMR spectra of the DPPDI-R3.

zxj20160311-1

273-1



273-1

ZXJ160317-4-C

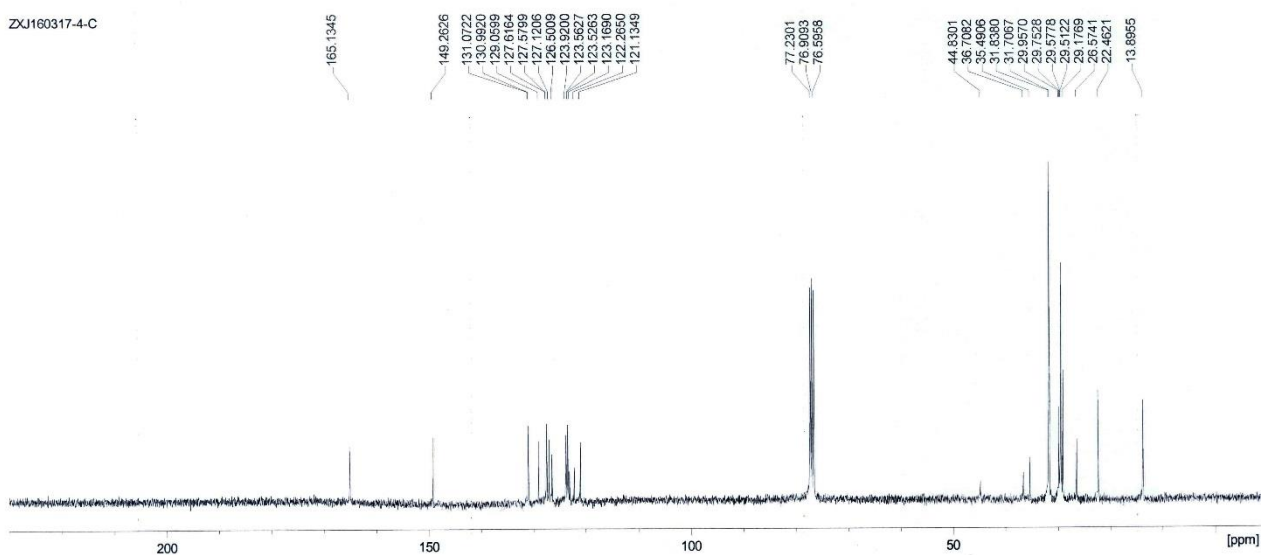
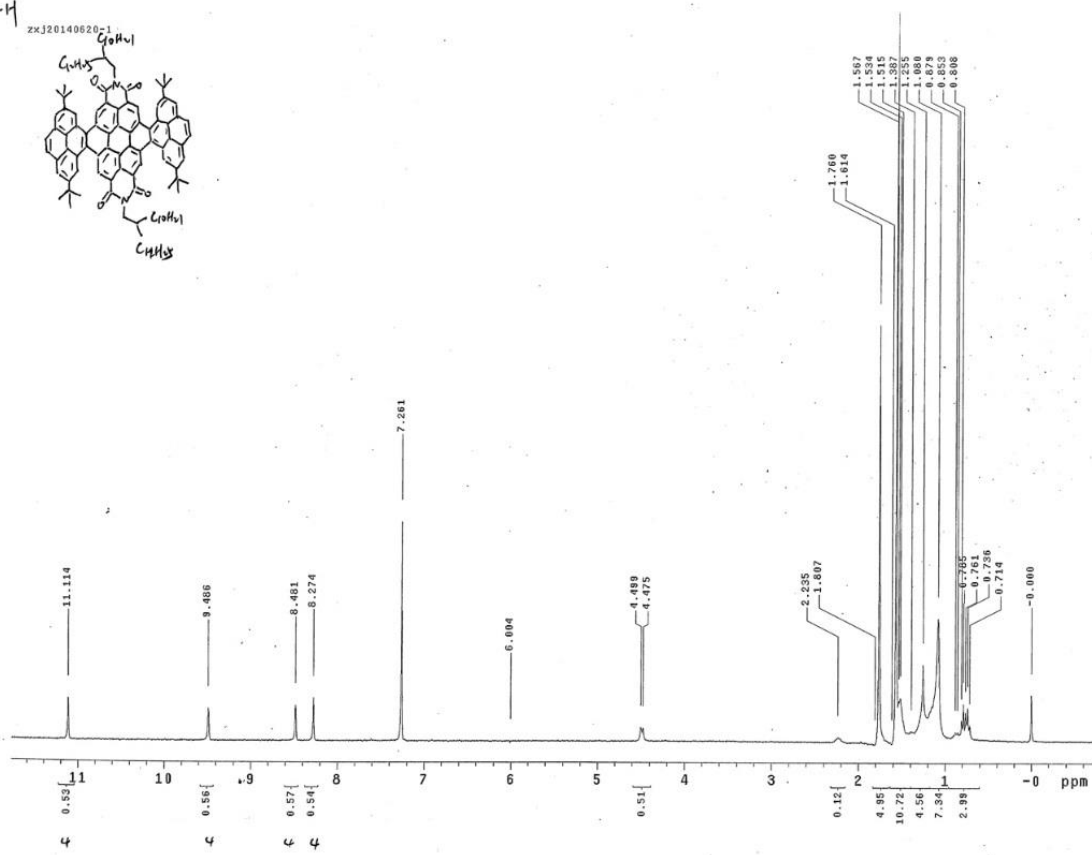
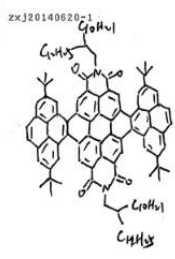


Figure S10. ^1H NMR and ^{13}C NMR spectra of the DPPDI-R4.

201-1-1



201-1-C

ZXJ140630-201-C

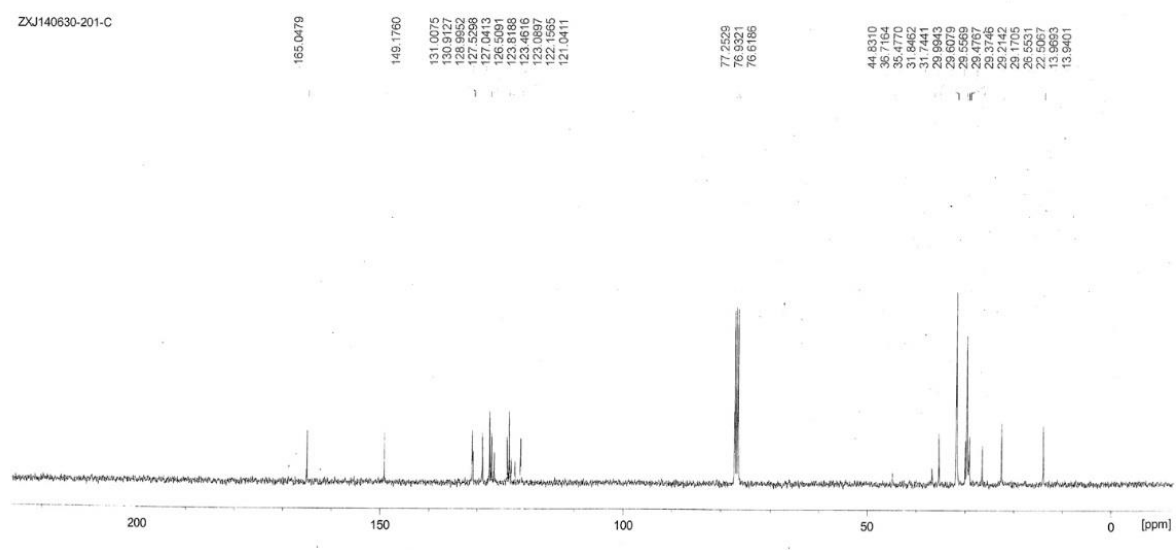
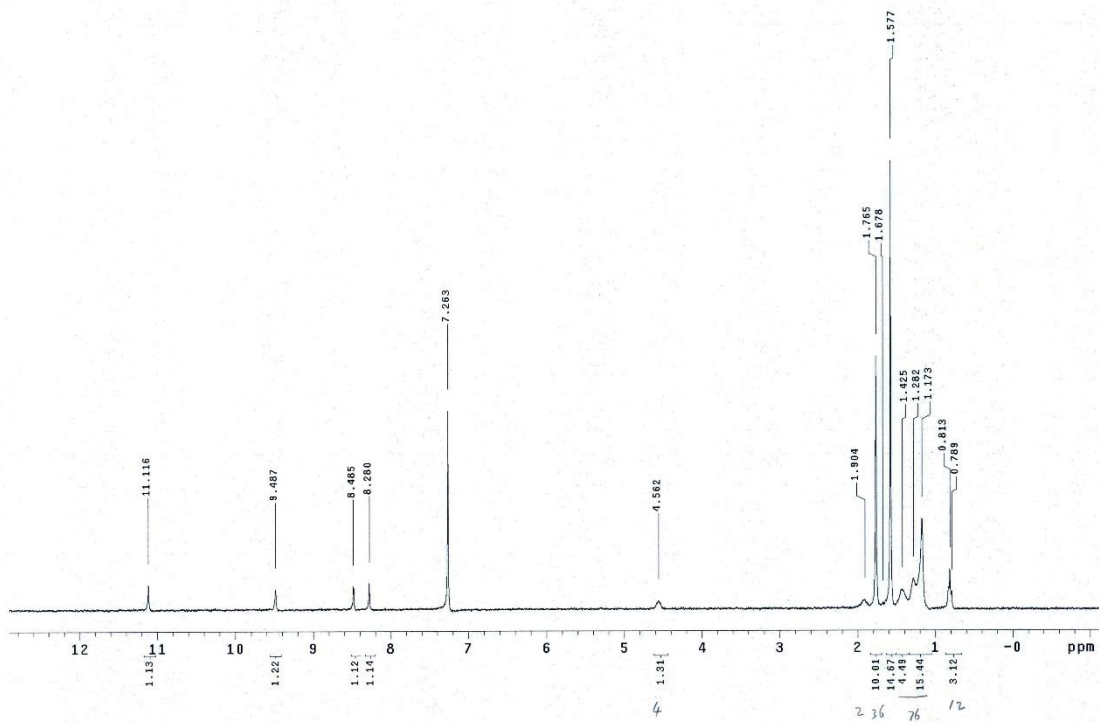


Figure S11. ¹H NMR and ¹³C NMR spectra of the DPPDI-R5.

ZXJ20160309-272-1



ZXJ160323-6-C

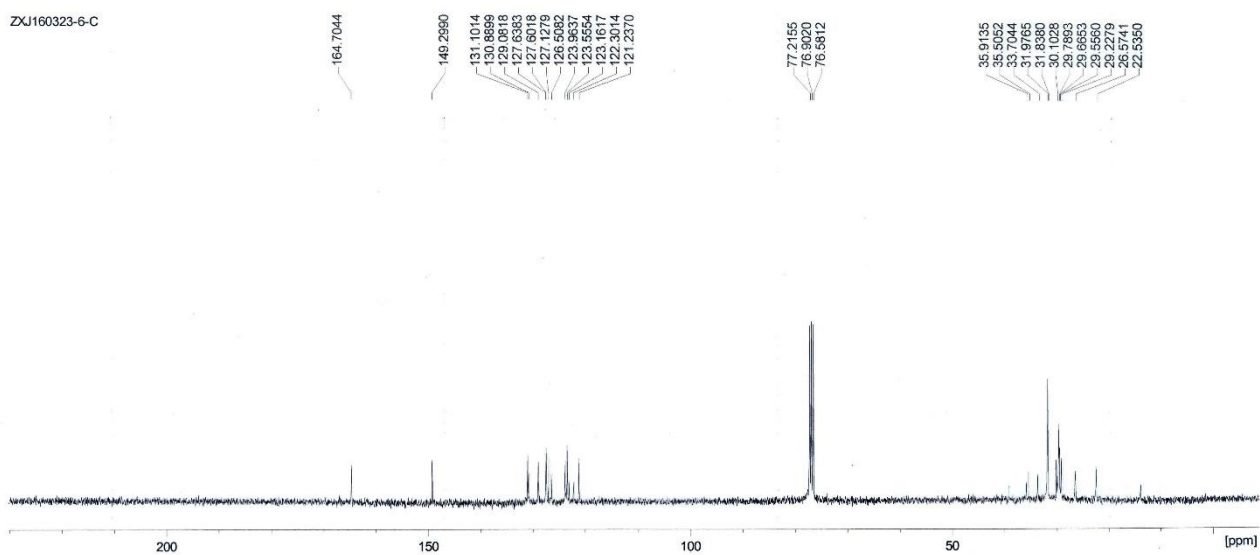


Figure S12. ^1H NMR and ^{13}C NMR spectra of the DPPDI-R6.

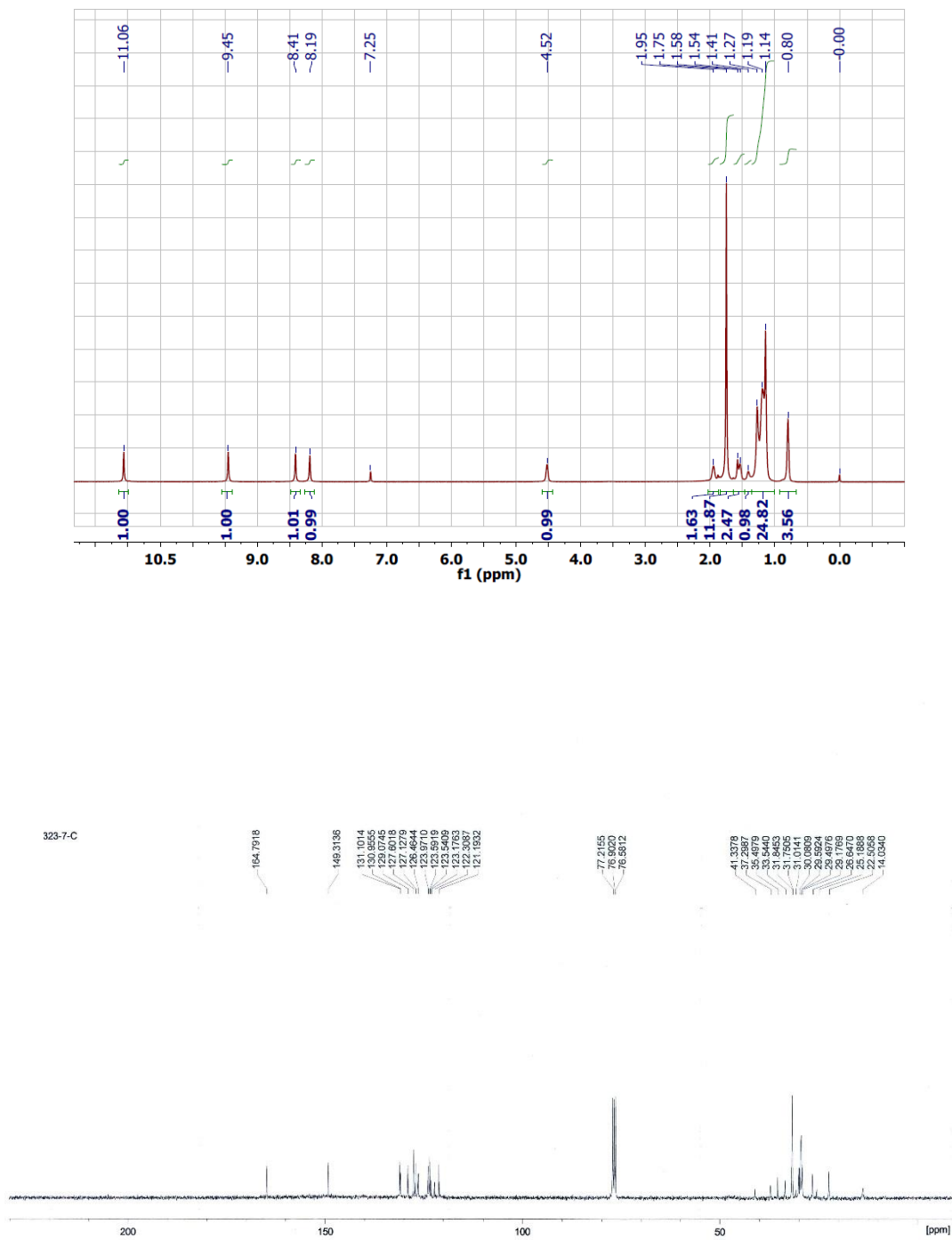
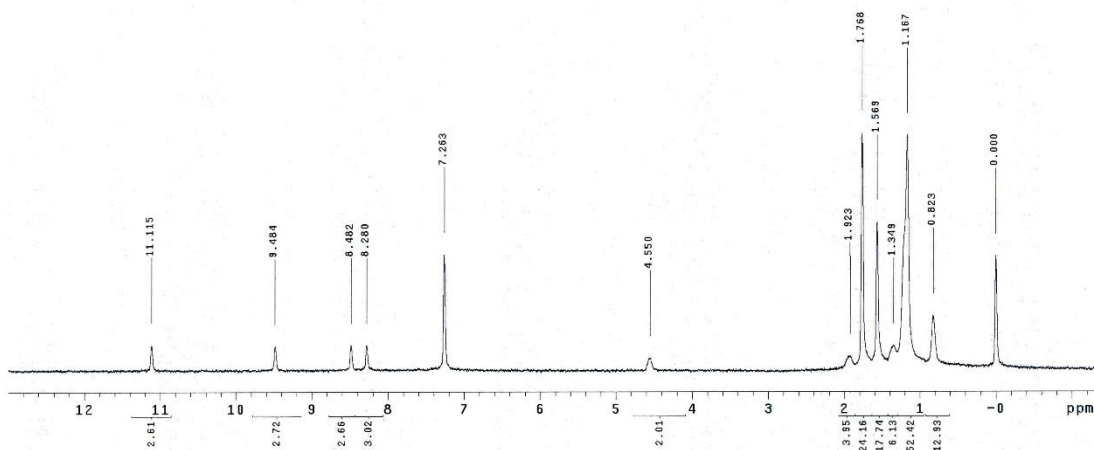


Figure S13. ¹H NMR and ¹³C NMR spectra of the DPPDI-R7.

7/3-1



1.85-1

ZXJ160330-8-C

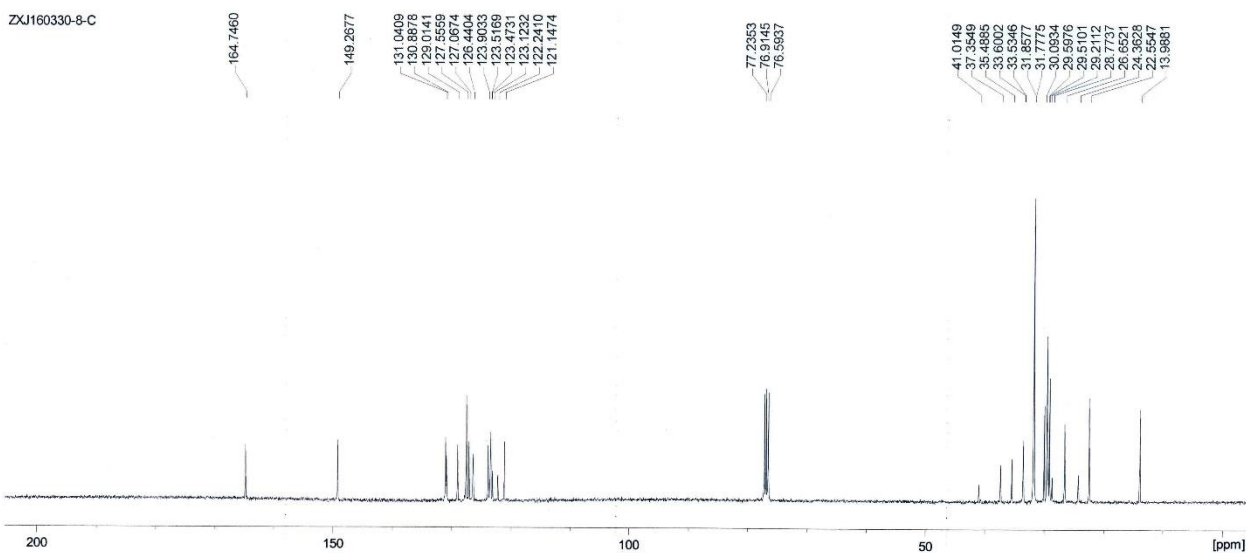


Figure S14. ¹H NMR and ¹³C NMR spectra of the DPPDI-R8.

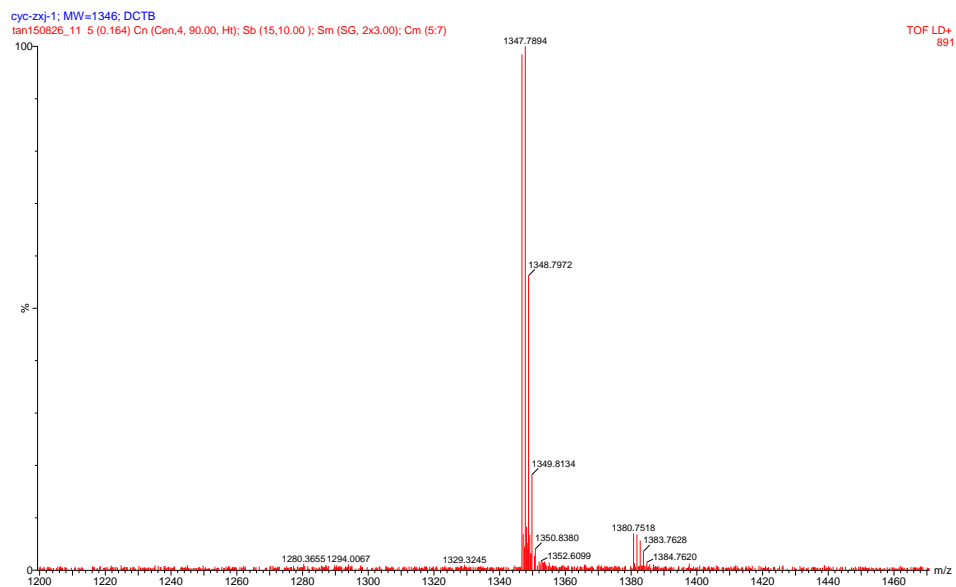


Figure S15. HRMS (MALDI-TOF) spectrum of DPPDI-R1.

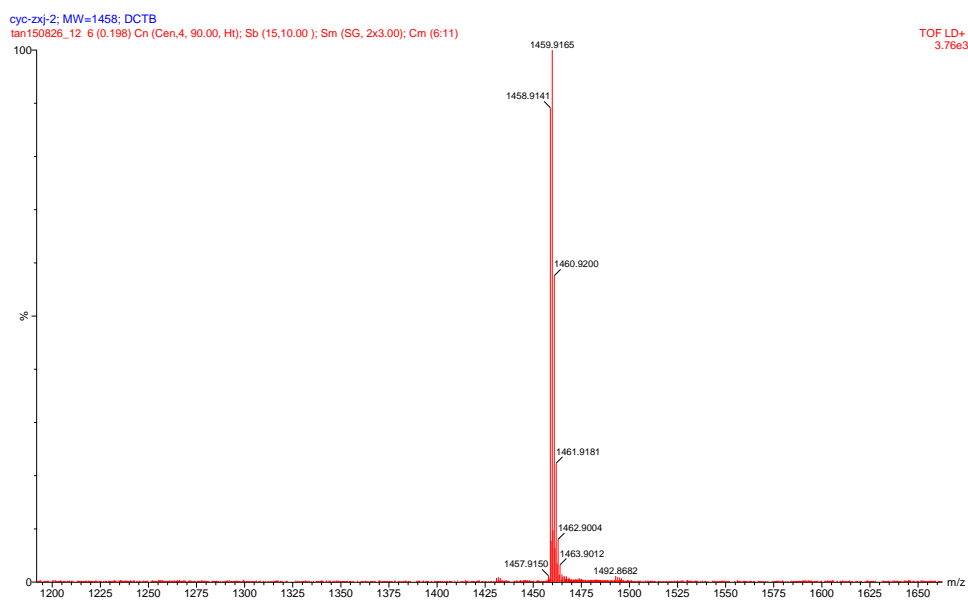


Figure S16. HRMS (MALDI-TOF) spectrum of DPPDI-R2.

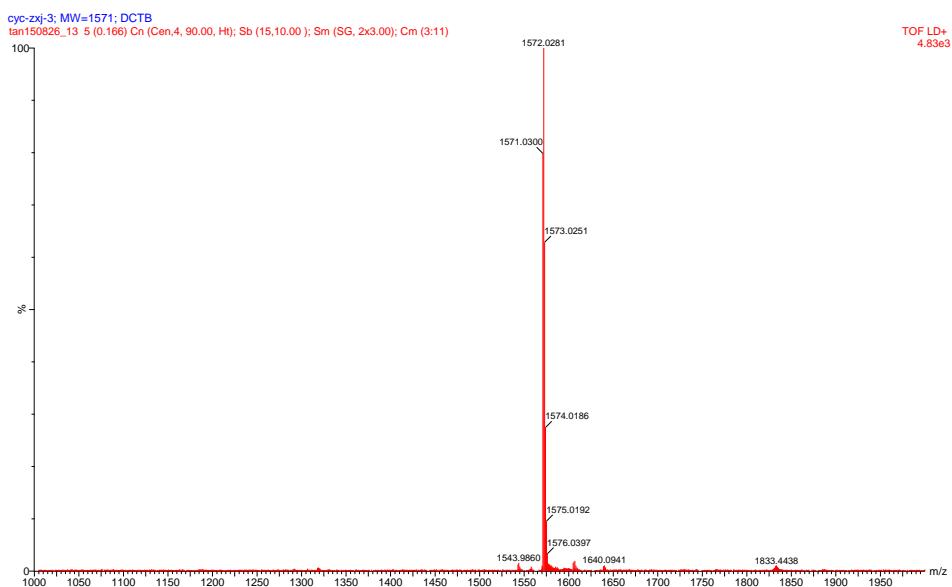


Figure S17. HRMS (MALDI-TOF) spectrum of DPPDI-R3.

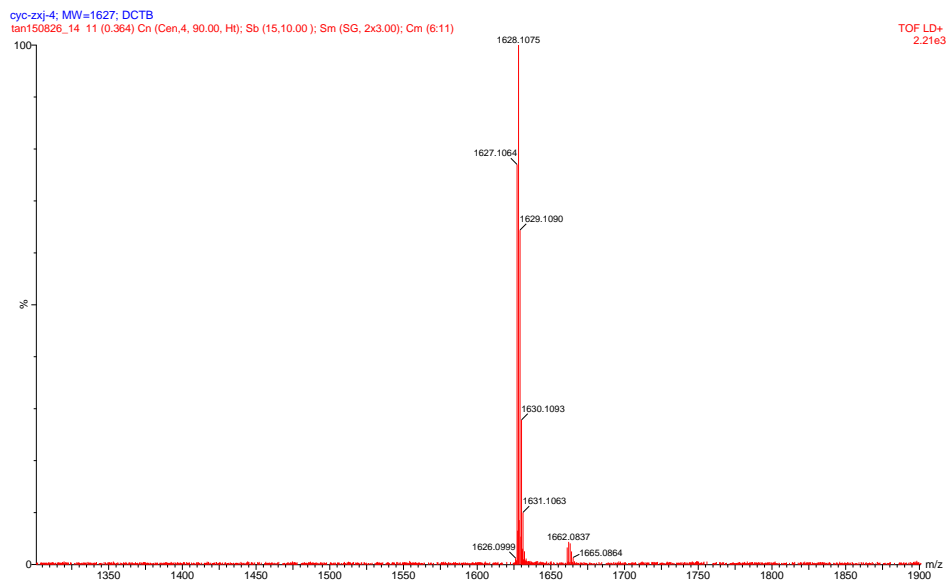


Figure S18. HRMS (MALDI-TOF) spectrum of DPPDI-R4.

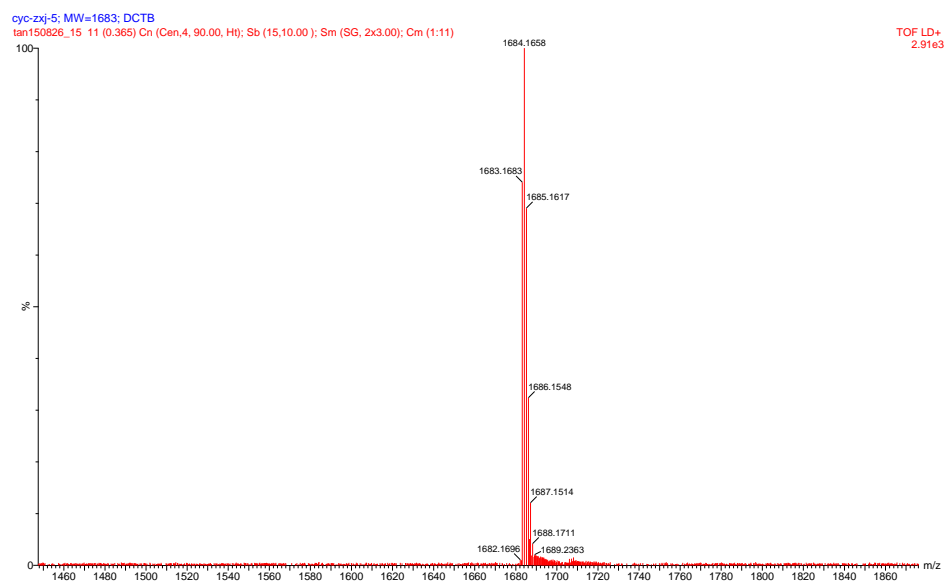


Figure S19. HRMS (MALDI-TOF) spectrum of DPPDI-R5.

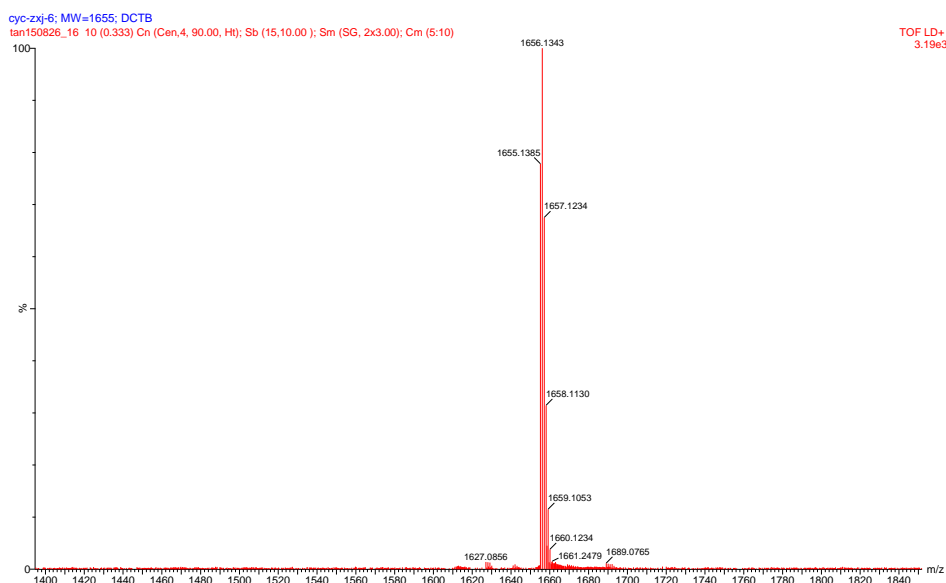


Figure S20. HRMS (MALDI-TOF) spectrum of DPPDI-R6.

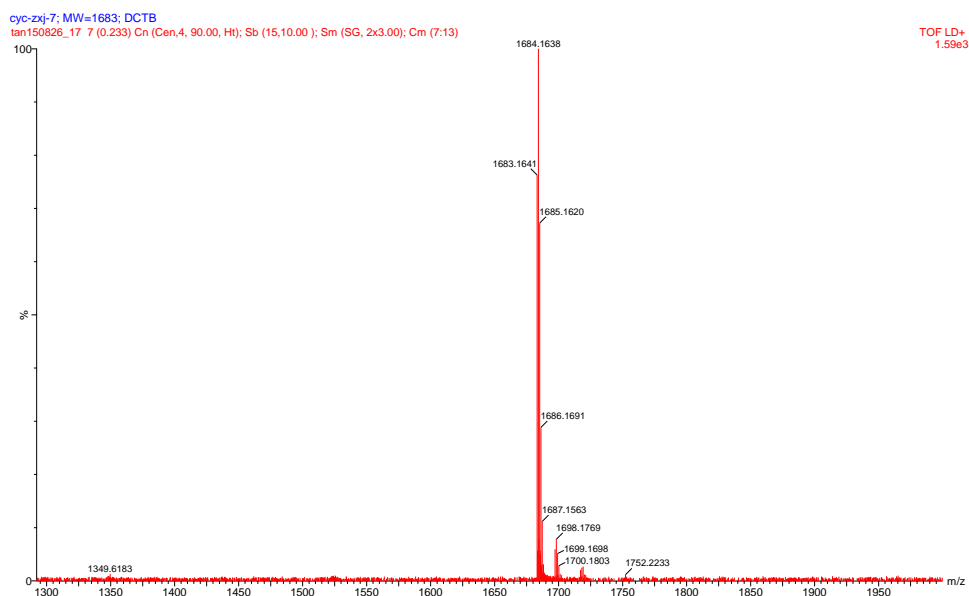


Figure S21. HRMS (MALDI-TOF) spectrum of DPPDI-R7.

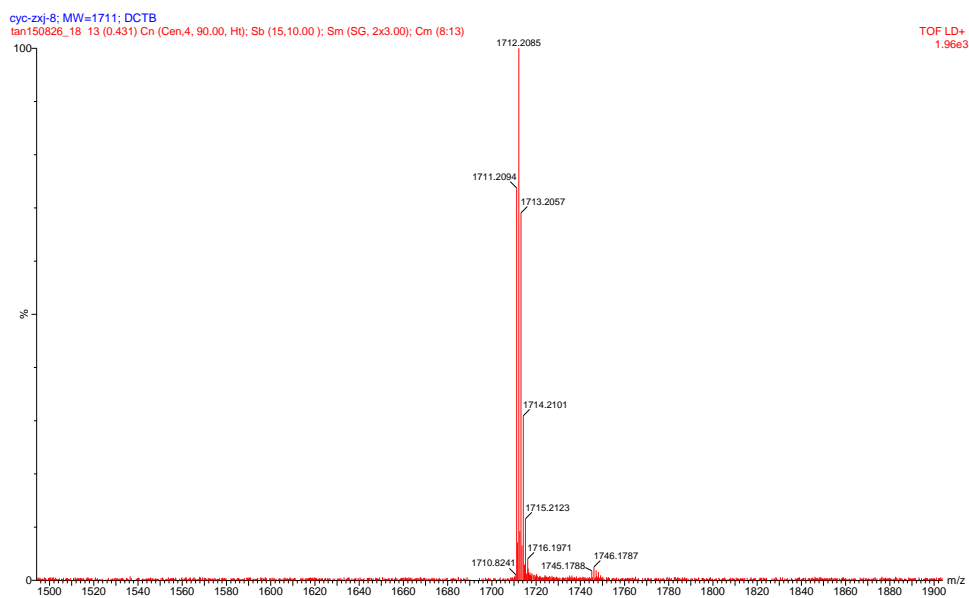


Figure S22. HRMS (MALDI-TOF) spectrum of DPPDI-R8.